Scientia Iranica A (2022) 29(6), 2902–2918

Sharif University of Technology
Scientia Iranica
Transactions A: Civil Engineering
http://scientiairanica.sharif.edu

Dynamic analysis of reinforced concrete water tanks under blast considering fluid-structure interaction

M. Moghadam, S.V. Razavitosee*, and M. Shahrbanouzadeh

Department of Civil Engineering, Jundi-shapur University of Technology, Dezful, Iran.

Received 27 March 2021; received in revised form 18 September 2021; accepted 7 March 2022

KEYWORDS
Dynamic response;
Water tanks;
Blast loading;
Hoop stresses;
Tank wall displacement;
Water-structure interaction.

Abstract. This study investigates the blast effect on hoop stresses and displacements created on the wall of over-ground cylindrical reinforced concrete water tanks and the effects of blast waves, fluid surface motion, and the surface tension of water due to water-structure interaction using ABAQUS software. Three water tanks with heights of 4, 6, and 8 m and a fixed radius of 3 m were used for simulation, each of which was filled with 0, 25, 50, 75, and 100% water from the depth of the tank. The results revealed that the above parameters affect the water tank structure's dynamic response so that the surface tension of water is higher in water tanks with 50% water filling. Also, increasing the water filling percentage, the hardness of the water tank increased and decreased the tank wall displacement by 31.25% for a filled water tank compared to an empty water tank. The results illustrate that the water tank wall's hoop stresses were affected by blast waves from the outside and water tension from the inside, so that the water tension in the water tank caused an approximate 20 MPa increase in the hoop stresses on the wall.

1. Introduction

Generally, water tanks are characterized as essential components of water supply systems. The water tanks are designed based on different aspects, including compensating for changes in water demand; reducing water pressure fluctuations in distribution networks; storing and providing the required water for firefighting; continuity of water supply or distribution during power outages or hazardous incidents; and preventing water pollution. The storage of drinking water is affected by several factors: proper design, selection of materials, and the construction and maintenance of the water tanks. Population growth, urban development, and the high living standards of citizens have forced the governments to construct numerous water tanks in different parts of the country to meet water supply demands. Therefore, the design and calculation of these water tanks are performed based on the latest national and international standards to ensure the efficiency of these infrastructure facilities [1]. Also, it is essential to investigate the behavior of structures considering the influence of this type of loading. This issue is due to the spread of terrorist attacks and blasts caused by large-load and concentrated explosives on structures. The present study evaluates the strength of water tanks considering several phenomena, comprising the effect of water-structure interaction in an explosion and blast loading; the specific influence of water turbulence force; and the effect of water-structure interaction on the stresses of the water tank structure. The study of water-structure interaction plays a crucial role in analyzing water-related structures in response to

*. *Corresponding author. Tel.: +98 9226261737*
E-mail address: vrazavi@jsu.ac.ir (S.V. Razavitosee)

doi: 10.24200/sci.2022.57932.5478

dynamic force. In this case, water is presumed to be a continuous, incompressible, and non-rotating medium. The motion equations are configured in the water tank environment based on the governing differential equation. Thus, the hydrodynamic waves and their corresponding boundary conditions are propagated (i.e., forming the Laplace equation) [2].

Over the years, many researchers have studied earthquake-stimulated fluid water tanks [3–6]. The preliminary studies on water tanks have been performed by assuming a rigid wall and two linear and nonlinear behavior modes for the liquid. Hoskins and Jacobsen (1934) [7] investigated the influence of hydrodynamic pressure on rectangular water tanks subjected to horizontal stimulation. They have focused on analyzing and evaluating rigid-wall cylindrical water tanks. Housner [8] modeled a rigid cylindrical and rectangular water tank for the practical use of civil engineers. In this model, the liquid pressure has been divided into two parts: the impulsive component caused by the movement of a portion of the liquid with an acceleration equivalent to the wall acceleration and the convective component obtained by liquid sloshing. Epstin [9] determined the maximum forces caused by an earthquake. The values have been computed using a series of equations and tables and assuming that the convective component acts on the upper part of the liquid. Haroun [10] proposed a new model for the water tank-liquid system using the finite element method, boundary solution, and computer programming. In this model, the effect of higher modes of cos $n\theta$ has been considered in addition to the influence of cos θ type mode. In 1984, Veletsos modeled water tanks with flexible walls [11]. This process has been performed via substituting the quasi-acceleration function by the ground acceleration of the impulsive component of rigid-wall water tanks. Ormeño et al. [12] suggested several seismic ground motion scaling methods for the dynamic analysis of water tanks. Ruiz et al. [13] proposed an efficient computational methodology for seismic analysis of water tanks. The proposed model revolves around the theory of potential flow. In this case, the continuity equation is solved through the finite element method. Javanmardi et al. [14] applied the computational fluid dynamic approach to analyze the water moving pressure act and the channel parameters on the generated waves in the channel. They demonstrated that the enlargement of the draft has led to the increment of the angle of attack, the beam of the pressure source, and the height of the generated wave. Zhang et al. [15] employed the Arbitrary Lagrangian-Eulerian (ALE) method to evaluate the coupling responses of water and aqueducts with high bent-type under wind loads. They proved that the isolated support altered the dynamic properties and reduced the wind resistance performance of the U-shape aqueduct. Brunesi et al. [16] assessed the dynamic reaction of cylindrical water tanks based on field observations. The data was gathered during the May 2012 earthquakes in northern Italy. They found that the large majority of cylindrical water tanks were severely damaged. Colombo and Almazán (2015) [17] utilized the seismic capability method to evaluate the performance of a specific energy dissipation method in two narrow and wide cylindrical water tanks. Jin et al. [18] applied a numerical model to investigate the sloshing hydrodynamic properties and the pressure response in a two-dimensional rectangular water tank. They introduced an adequate baffle system for all seismic excitations based on dynamic analysis.

Most previous research considered seismic force as a dynamic effect on water tanks. However, it is necessary to investigate the dynamic effects of the structures exposed to the blast loadings. Analyzing the effect of blast loading on structures has begun since the 1960s. In 1959, the US Army published a journal paper entitled "Blast-resistant Structure". The publication was edited in 1990. The edited version has widely been applied by military and civilian organizations to design structures, prevent the spread of explosions, and protect military equipment and personnel [19]. Then, several numerical and laboratory studies on the blast in various structures, such as water tanks, were completed [20,21]. For example, Wang et al. [22] reported that a straightforward designed water tank had a blast resistance smaller than a reinforced water tank. This situation occurs only by increasing the internal energy and decreasing the external work (through adopting limited axial boundary conditions). Mittal et al. [23] utilized the coupled Euler-Lagrange formula to assess the dynamic analysis of water tanks under blast loading. They discovered that increasing the liquid height in the water tank, decreasing the scale distance of explosives, increasing the ratio of dimensions, and increasing the ratio of height to radius could all increase stresses. Hu and Zhao [24] utilized fluent software to model a small-scale water tank under blast loading. The achieved results have been validated by a laboratory sample. They investigated the internal pressure distribution in the water tank according to several factors, including the water tank capacity, the ratio of height to depth, and the shape of the water tank roof. Zhang et al. [25] employed a numerical method to analyze a gas tank considering the effect of TNT blast loading. They also calculated the resulting pressure and deformation. Lee et al. [26] and Li and Hao [27] examined the blast pressure inside and outside the space of the water tanks. They presented the calculation procedure for the internal and external pressures in the water tanks. In this case, LS-DYNA software has been employed to express the different distances between the water tanks. Lu et al. [28] modeled the effect of a blast

on a cylindrical metal water tank and then compared the results with a laboratory sample. They also evaluated the generated fracture mode, deformation, energy, and dynamic strain. Yasseri [29] performed some laboratory studies to introduce an equation for water tanks with a height lower than the diameter. This procedure has been performed to obtain the distribution of external blast pressure around the water tanks under vertical pressure. Safa [30] implemented a nonlinear dynamic analysis for groundwater tanks with floating roofs under the blast load. In this case, the analysis process has been carried out for 30 different blast loading modes. The results showed that the bodies of the water tanks were vulnerable in some blast loading scenarios, and the damage took place according to the failure criteria of the API650 design code. Wang and Zhao employed a numerical analysis and demonstrated that water could reduce the response of the water tank subjected to blast loading [31]. The investigation was carried out for two modes of a metal water tank, taking into account simple and limited support in the structure's axis. They demonstrated that in a water tank with limited support conditions in the axis, internal energy increased while external work decreased.

Several types of research have been performed on water tanks under dynamic loads (e.g., earthquakes and blasts on metal water tanks), and their results have provided valuable information. However, there is a gap concerning the study of the behavior and response of the reinforced concrete over-ground water tanks under the blast, assuming the water-structure interaction. In this regard, the coupled Euler-Lagrange equation has been employed in ABAQUS software [32]. Then, the obtained results have been utilized to determine the stresses caused by the external blast and internal water pressure against the parameters affecting the behavior of the structure. In the present study, three reinforced concrete water tanks with different heights of 4, 6, and 8 m and a fixed radius of 3 m have been considered. Each one contains 0, 25, 50, 75, and 100% water from the depth of the water tank. In this case, the hoop stresses of the water tank wall and the fluid surface motion induced by blast loading have been investigated.

2. Method

On the water tank walls, 94 grade-10 rebars are perpendicular, and in every 1 m height, five grade-8 rebars circularly surround the vertical rebars. These bars are buried inside the concrete. Figure 1(a) shows how the rebars are attached, and Figure 1(b) shows the concrete wall.

2.1. Concrete

Concrete is one of the materials whose failure level depends on hydrostatic pressure. Different criteria have been proposed for concrete, one of which is the criterion for yielding concrete, plastic damage, dependent on the hydrostatic pressure in concrete modeling. To predict the nonlinear behavior of concrete and consider the effects of the decline in the concrete strength due to failure, the damaged plasticity model for concrete is used, where the compressive and tensile behavior of concrete and the two parameters of compressive damage and tensile damage are considered. This model uses the concept of isotropic damage in the linear range and shows the nonlinear behavior of concrete by combining isotropic tension and plastic pressure. The elastic and plastic properties of concrete defined in this research are given in Table 1.

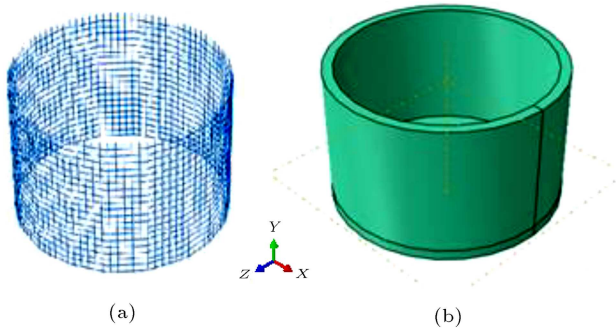

(a) (b)

Figure 1. Reinforced concrete water tanks: (a) Rebars and (b) concrete.

Table 1. Elastic and plastic characteristics of concrete [33].

No.	Features	Value
1	Dilation angle, ψ (degree)	31
2	Eccentricity, ε	0.1
3	f_{b0}/f_{c0}	1.16
4	Second stress invariant, k	0.666
5	Viscosity (N.s/m^2)	0.0001
6	Density (kg/m^3)	2450
7	Young's modulus (N/m^2)	235E8
8	Poisson's ratio, υ	0.2

In Table 2, concrete compressive and tensile behavior is assigned to concrete in the material module of ABAQUS software.

2.2. Rebar

Steel is used to model reinforcements in concrete. Since blast loads usually produce incredibly high strain rates in the range of $10^2 \sim 10^4$ s^{-1}, they change the mechanical properties of materials in the structure and the expected mechanisms. According to Table 3, the plastic properties of the steel have been assumed using the Johnson-Cook hardening model to consider the impact of strain rate on the stress. According

Table 2. Compressive and tensile behavior of concrete ABAQUS [33].

No.	Compressive behavior		Tensile behavior	
	Yeild stress (Pa)	Inelasic strain	Yeild stress (Pa)	Cracking strain
1	20480000	0	3200000	0
2	24000000	6.88E-005	320000	0.00119
3	26880000	0.000161		
4	29120000	0.000278		
5	30720000	0.0004184		
6	31680000	0.0005826		
7	32000000	0.00077		
8	31680000	0.000982		
9	30720000	0.00122		
10	29120000	0.00148		
11	26880000	0.00176		
12	24000000	0.00207		
13	20480000	0.0024		
14	16320000	0.00275		
15	11520000	0.00313		

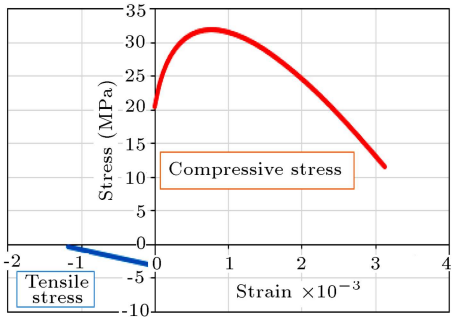

Table 3. Johnson-Cook model specifications [34].

No.	Variable	Value
1	A (MPa)	360
2	B (MPa)	635
3	N	1.03
4	M	0.114
5	Melting temperature (K)	1500
6	Transition temperature (K)	298
7	C	0.075
8	Epsilon dot zero	1

to Eq. (1), stress is defined as a function of plastic strain, strain rate, and temperature in the Johnson-Cook model [23]. This feature is easily defined in the ABAQUS software:

$$\sigma = (A + B\varepsilon^n)(1 + C\ \log_e \varepsilon^*)(1 - T^{*m}), \qquad (1)$$

where $\varepsilon^* = \frac{\dot{\varepsilon}}{\dot{\varepsilon}_0}$ is the dimensionless plastic strain rate in the reference strain rate $\varepsilon_0 = \frac{1}{S}$, and $\dot{\varepsilon}$ is equal to the plastic strain rate; T^* is the corresponding dimensionless temperature; A is the initial rupture strength of steel at a plastic strain rate of $\dot{\varepsilon} = \frac{1}{S}$, and the temperature is 298 Kelvin; B and n simulate the hardening behavior of steel independent of the strain rate; and C reflects the hardening behavior dependent on the strain rate; and m is the thermal softening coefficient obtained for steel from mechanical tests and is equal to 0.114. The specifications of the Johnson-Cook model for rebar are given in Table 3.

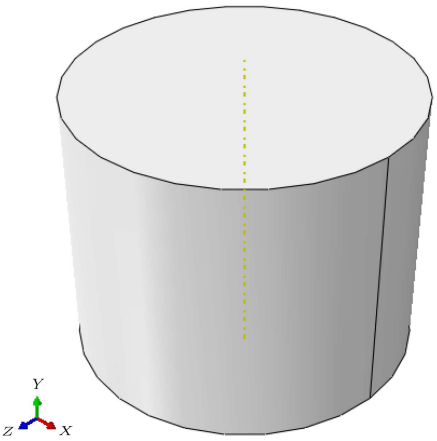

Figure 2. Geometric shape of the fluid inside the water tank.

2.3. Fluid

The fluid in the tanks is water. Each water tank, depending on its water height, covers 0, 25, 50, 75, and 100% of its volume with fluid. Figure 2 shows the fluid inside the water tank.

2.3.1. Coupled Euler-Lagrange (CEL) formula

The Coupled Euler-Lagrange (CEL) formula analysis allows modeling of the Euler-Lagrange interaction domains in one model. This analysis is typically used to model the interactions of a solid and a fluid. Therefore, in the CEL method, the Euler material can contact the Lagrange, known as the Euler-Lagrange contact. Therefore, this powerful tool makes it possible to model many multi-phase problems, including fluid-structure contact. Because of Eulerian fluid modeling, the problems caused by large deformations of the

fluid have been eliminated. In the so-called method, the fluid elements are fixed in the space, and the fluid flows smoothly inside them; the water tank structure is defined in this method as the Lagrangian formulation. Since the implementation of the Euler method in ABAQUS software is based on the fluid volume method, in this method, the position of the Euler material in the mesh environment is determined by calculating the volume fractions of Euler in each element. By this definition, if an element is filled with a substance, its Euler volume fraction is one, and if no substance is included in it, its Euler volume fraction is zero [21].

2.3.2. Fluid properties in ABAQUS

In turbulence issues, the fluid can be considered incompressible and non-viscous. A practical method for fluid modeling in ABAQUS/explicit is to use the Newtonian shear viscosity model and the $U_S - U_P$ linear equation. The bulk functions act as correction parameters for fluid incompressibility constraints. Since the turbulence of the fluid inside the water tank is free and unconstrained, the bulk modulus can be considered two to three times smaller than the actual value, and the fluid can still behave in an incompressible way. The shear viscosity acts as a corrective parameter to neutralize the shear modes that cause mesh failure. Because water is a non-viscous fluid, the shear viscosity of the fluid must be considered small. High shear viscosity results in highly rigid responses. The value of suitable viscosity can be calculated based on the value of the bulk modulus [21].

2.3.3. Energy equation and Hugoniot curve

The energy equation in the absence of heat transfer is written as Eq. (2):

$$\rho \frac{\partial E_m}{\partial t} = (P - P_{bv}) \frac{1}{\rho} \frac{\partial \rho}{\partial t} + S : \dot{e} + \rho \dot{Q}, \tag{2}$$

where P is the pressure; P_{bv} is the pressure due to the viscosity of the fluid; S is the deviatoric stress tensor; $\dot{e}$ is the deviatoric part of the strain rate; $\dot{Q}$ is the heat rate per unit mass, and E_m is the internal energy per unit mass. The equation of state is a function of density ρ and internal energy per unit E_m mass. Eq. (2) can define all the equilibrium states that exist in an object. Internal energy can be omitted from the above equation to obtain the relation between ρ and V or its equivalent ρ and $\frac{1}{\rho}$. The relationship between ρ and $\frac{1}{\rho}$ is called the Hugoniot curve [21].

$$P = f(\rho E_m). \tag{3}$$

Figure 3 schematically shows the Hugoniot curve; the Hugoniot pressure P_H is only a function of density, and the curve is generally plotted by processing experimental data [21].

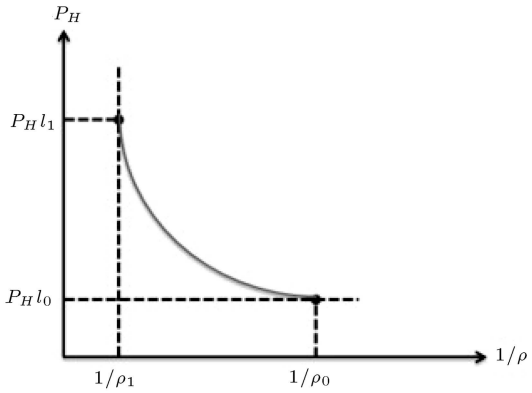

Figure 3. The Hugoniot curve for pressure-time relationship definition [21].

2.3.4. State equation Mie-Grüneisen

In the Mie-Grüneisen equation, the energy is linear. Its standard form is given in Eq. (4):

$$P - P_H = \Gamma \rho (E_m - E_H), \tag{4}$$

where P_H and E_H are the specific pressure and the specific energy of Hugoniot per unit mass, respectively, and Γ is the Grüneisen coefficient. The Grüneisen coefficient is calculated using Eq. (5). The specific pressure and the specific energy of Hugoniot are only functions of density.

$$\Gamma = \Gamma_0 \frac{\rho_0}{\rho}. \tag{5}$$

In Eq. (5), Γ_0 is the constant of matter, and ρ_0 is the reference density. The energy of Hugoniot E_H is dependent on the Hugoniot pressure and is obtained using Eq. (6):

$$E_H = \frac{P_H \eta}{2\rho_0}, \tag{6}$$

where $\eta = 1 - \frac{\rho_0}{\rho}$ is a function of current density ρ. By placing Eqs. (5) and (6) in Eq. (4), the Mie-Grüneisen equation of state is obtained as Eq. (7):

$$P = P_H \left(1 - \frac{\Gamma_0 \eta}{2}\right) + \Gamma_0 \rho_0 E_m. \tag{7}$$

2.3.5. Linear Hugoniot $U_s - U_p$

The P_H equation is shown by processing the Hugoniot information in Eq. (8):

$$P_H = \frac{\rho_0 C_0^2 \eta}{(1 - S\eta)^2}. \tag{8}$$

In this relation, S and C_0 create a linear relationship between the U_S impulsive velocity and the U_P particle velocity according to Eq. (9):

$$U_S = C_0 + S U_P. \tag{9}$$

S and C_0 are the slope of the Hugoniot curve and the velocity of the sound wave in water, respectively. The

Table 4. The specifications of the tank water [23].

No.	Variable	Value
1	Density (kg/m^3)	1000
2	Viscosity (N.s/m^2)	0.001
3	Sound velocity in water (m/s)	1450
4	Curve slope	0

velocity of the sound wave in water is calculated by Eq. (10):

$$C_0 = \sqrt{\frac{K}{\rho}}. \tag{10}$$

In this relation, K is the modulus of the fluid bulk, and ρ is the density of the fluid. According to the above relations, the linear form of Hugoniot is presented as Eq. (11):

$$P = \frac{\rho_0 C_0^2 \eta}{(1 - S\eta)^2}\left(1 - \frac{\Gamma_0 \eta}{2}\right) + \Gamma_0 \rho_0 E_M. \tag{11}$$

According to the ABAQUS software guide, the value of S, the slope of the curve and Γ_0, and the Grüneisen coefficient for water are considered equal to zero. The specifications of the water tank are given in Table 4.

2.4. Blast loading

In general, there are two types of perspectives for modeling blast loading in structures: (a) blast loading in the form of pressure-time history applied to all or some parts of the structure without considering the effect of the structural deformation on the pressure distribution and (b) loading with complete modeling of the structural and fluid environment as a complete coupling. The second method, if implemented correctly, leads to much more accurate results than the first method. However, it is very complex, and the analysis takes a much longer time. The first method is modeled by conventional finite element software. But the second method is not modeled and analyzed by many of the available software packages. Besides, the adjustment of the second method is complex and time-consuming in available software packages. Many blast loadings are derived as a decent approximation of the blast of a spherical charge.

Overall, blast load is applied to the concrete water tanks using the pressure-time history curve. Figure 2 shows the pressure-time curve for a blast wave in the open environment. As shown in this figure, it is divided into positive and negative phases. This procedure is often considered in analyzing and designing blast-resistant structures. In this case, the negative phase is less critical than the positive phase. This issue is due to its low blast pressure (suction). The rapid increase in pressure is either called the positive phase or the over-

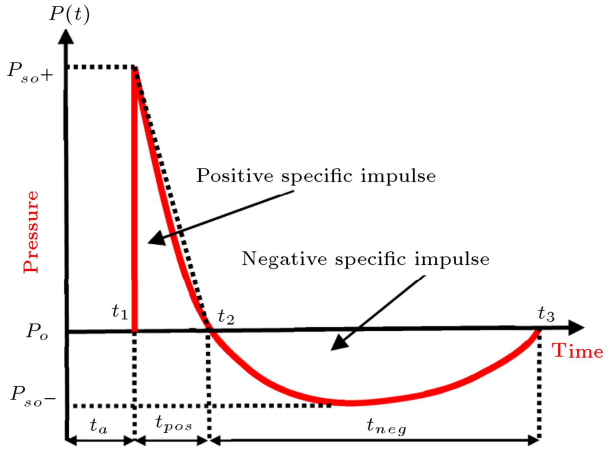

Figure 4. Pressure-time for blast waves in the air [12].

pressure phase. In this phase, the maximum pressure ($p_{s_0}^+$) is formed immediately after reaching the blast pressure on the structure (t_a) and returning to the atmospheric pressure (p_0) during the holding time (t_d). In the negative phase, the pressure first decreases and then increases and returns to the atmospheric pressure (p_0) during the holding time (t_d^-). The pressure-time curve in Figure 4 is described by Eq. (12) and using the Friedlander modified equation (Eq. (12)):

$$P(t) = p_{s_0}^+ \left(1 - \frac{t}{t_d^+}\right)^{\left(\frac{-b(t-t_a)}{t_d^+}\right)}. \tag{12}$$

In this relation, $P(t)$ indicates the intensity of the blast load on the water tank, and $p_{s_0}^+$ is the value of the blast pressure peak in MPa; t_a is the time of arrival of the blast wave in seconds; t_d^+ is the duration of the positive pressure in seconds, and b is a dimensionless value that controls the pressure drop [12].

One of the blast loading methods in ABAQUS software is the CONWEP method, in which the blast load is applied as a certain amount of TNT at a specific distance from the structure. The CONWEP model can be briefly defined using the free-explosion pressure-time diagram described by the modified Friedlander equation, expressed as Eq. (13) [12] :

$$\begin{aligned} &P(t) = P_i(t), \\ &\text{if :} \quad \cos\theta < 0, \\ &P(t) = P_i(t)\left(1 + \cos\theta - 2\cos^2\theta\right) + P_r(t)\cos^2\theta, \\ &f : \cos\theta \geq 0. \end{aligned} \tag{13}$$

In the above relation, $P(t)$ is the total compressive wave intensity on the adjacent structure at time t; $P_i(t)$ is the pressure of impulsive positive phase at time t; $P_r(t)$ is the reflective pressure at time t; and θ is the angle between the normal vector of the object surface and the vector that connects the collision surface to the

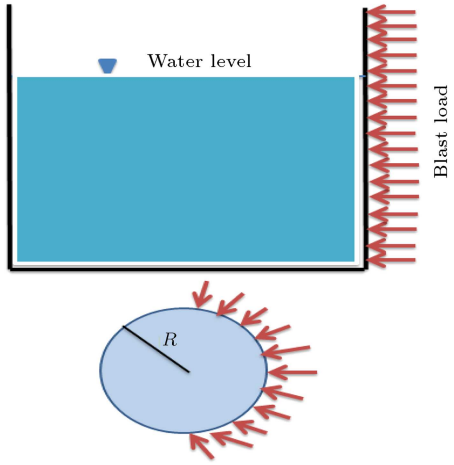

Figure 5. Blast load on the tank wall [12].

blast site [12]. The time the blast pressure reaches the water tank wall is shown in Figure 5. Increasing the amount of pressure on the structure is directly related to the distance and the number of explosives.

In this research, the CONWEP method has been used to apply an explosive load to the water tank. The type and mass of the explosion were airblast and 800 kg, respectively, from a distance of 10 m.

3. Meshing and sensitivity analysis

The importance of the convergence test is such that after the completion of the first analysis and evaluation of stress values and damage models in the mesh model, critical areas are identified. We set out to reach the optimal mesh size in critical areas by changing the mesh due to the sensitivity of these results to the defined mesh and the need to consider the time phases of the analysis and the optimal time spent. This optimal size for the mesh is created when the larger size affects the quality and quantity of the response, and the smaller size does not alter the response.

Luccioni et al. [35] studied the effect of the finite element mesh size used in commercial software to simulate and predict blast loads' responses. In this study, considering the importance of water-structure interaction, we examined the size of meshes from 30 cm to 3 cm (see Table 5). The results have shown that considering the meshing smaller than the A10 model

Table 5. The examined mesh sizes from 30 cm to 3 cm.

Hoop stress	Mesh size (cm)	Model name
5.53	30	A30
5.81	20	A20
5.92	10	A10
5.94	5	A5
5.95	3	A3

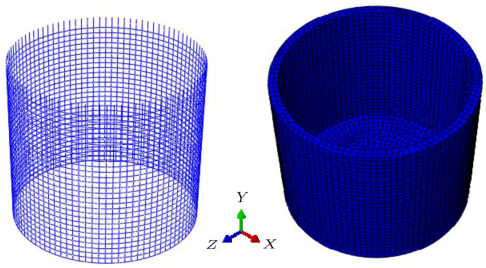

Figure 6. Optimal meshing used in current research.

with a mesh size of 10 cm, the hoop stress values in the tank change from 5.92 to 5.94 MPa. The researchers concluded that if a finite element mesh size of about 10 cm were selected, the blast loading process would be accurately modeled. Figure 6 shows the meshing of the water tank components at a size of 10 cm per piece. Also, information about the type of element, number of elements, nodes related to the tank, rebars, and water is shown in Tables 6 to 8, respectively.

4. Validation

The previous researches has been compared to evaluate the accuracy of the numerical modeling method used for applying blast loads on water structures (water tanks). Also, the CEL (Figure 7) has been used to validate the performance of the water tank based on water fluid-structure interaction. In this case, the blast loading on the structure implemented in ABAQUS software and the numerical modeling method represented by Mittal et al. have been compared and evaluated [12]. Steel water tanks with different dimensions and percentages of water fillings under 100 kg TNT blast have been analyzed at various distances from the water tank. Figure 8 depicts an overview of modeling these water tanks against the blast load. Also, the steel water tank specifications consist of the Johnson-Cook hardening model and Hugoniot equations for water. These specifications are modeled in ABAQUS software, and then the results are compared. Finally, the established model is validated.

In this case, a water tank with a 0.3 m height, 0.6 m radius, and 50% water filling under a 100 kg TNT blast at a distance of 2.35 m from the water tank has been modeled and assessed in ABAQUS software to confirm the validity of the model.

Figure 8 indicates the results derived from the hoop stress of the water tank body subjected to explosion. The wall hoop stress diagram is examined at the explosion peak and the pressures are applied to the water tank. In this regard, a path is selected from the edge of the wall to the floor. The path selection is carried out using the nodes of the water tank elements. In this case, its hoop stress value specifies every node, and its diagram is drawn. Table 9 compares the

Table 6. The type of element, number of elements, and nodes related to the tank.

Tank height (m)	No. of elements	No. of nodes	Element type
4	5297	8458	C3D8R
6	7505	11636	C3D8R
8	9822	14922	C3D8R

Table 7. The type of element, number of elements, and nodes related to rebars.

Tank height (m)	Rebar type				Element type
	Hoop rebars		Vertical rebars		
	No. of elements	No. of nodes	No. of elements	No. of nodes	
4	198	198	40	41	B31
6	198	198	60	61	B31
8	198	198	80	81	B31

Table 8. The type of element, number of elements and nodes related to water.

Tank height (m)	Tank filling (%)									
	0		25		50		75		100	
	No. of elements	No. of nodes	No. of elements	No. of nodes	No. of elements	No. of nodes	No. of elements	No. of nodes	No. of elements	No. of nodes
4	0	0	1407	2008	3293	4016	4470	5280	5811	6720
6	0	0	2345	3012	4470	5280	6735	7712	9720	10899
8	0	0	3283	4016	5811	6720	9720	10899	12042	13412
Element type	C3D8R		C3D8R		C3D8R		C3D8R		C3D8R	

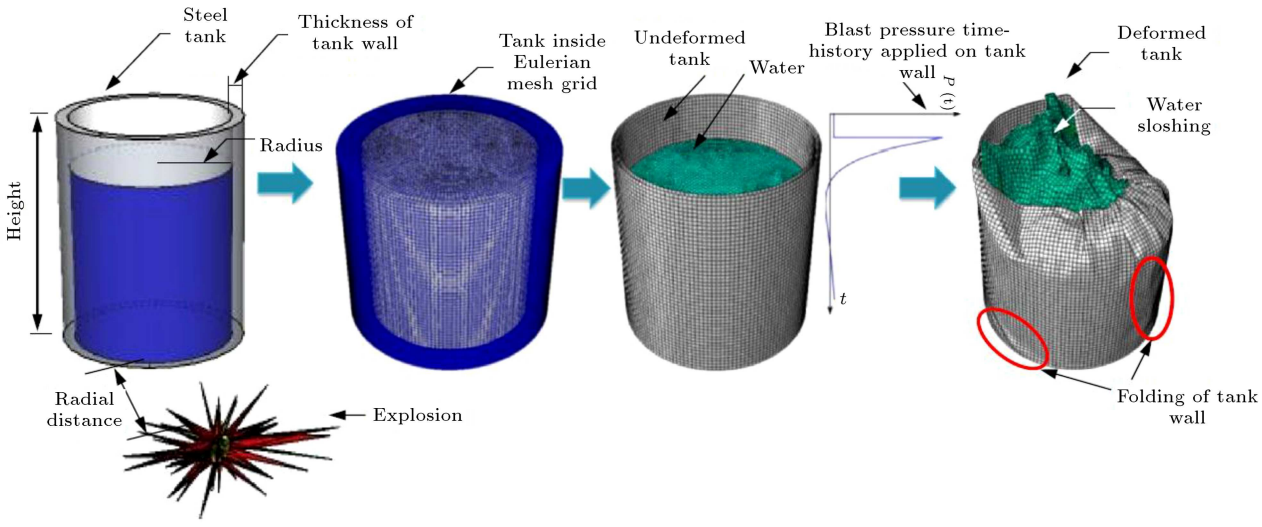

Figure 7. Steps in a coupled Euler-Lagrange simulation [12].

error percentage in the study performed by Mittal et al. [12] with the present study. The comparison results demonstrated that the difference value was less than 10%. Also, the average error was 5.9%, which was an acceptable value.

5. Results

The stability of the over-ground reinforced concrete cylindrical water tanks under blast has been investigated considering different modes such as the ratio

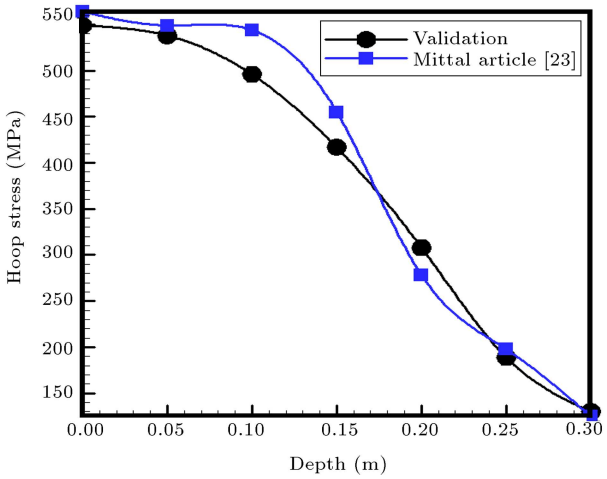

Figure 8. Comparison of hoop stress of the model with the research of Mittal et al. [23].

Table 9. The error percentage of [12] compared with the present study.

No.	Depth	Mittal	Research	Error (%)
1	0	549	564	2.73
2	0.05	538	546	1.49
3	0.1	496	544	9.67
4	0.15	417	455	9.11
5	0.2	308	278	9.74
6	0.25	189	198	4.76
7	0.3	130	125	3.84
Mean error (%)			5.90	

of height to the radius, different percentages of water in the tank, and different explosion distances. Also, the changes in a selected path on the water tank wall are considered to evaluate stresses and strains on the water tank wall. As shown in Figure 9, this path faces the explosion point and starts at point A and ends at point B. In the height path of the water tank, every node contains specific stress and strain, and ABAQUS software has been used to record the values in the path and display them in the form of a diagram. The vertical axis of these diagrams denotes the stress or strain created on the water tank wall, and their horizontal axis exhibits the height of the water tank.

5.1. Evaluation of the displacement of the water tank wall

Given that the blast waves are exerted directly onto the middle of the water tank body, assuming the height dimension by the CONWEP method, the waves are distributed up and down the water tank after blast loading. Figure 9 shows the selected paths on the wall against the explosion. It is selected from the highest node of the water tank wall to the bottom of the water tank. The nodes of the water tank wall elements are phased directly under the blast, and the phasing

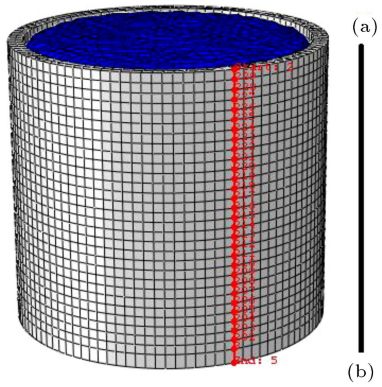

Figure 9. AB path on the wall facing the water tank blast.

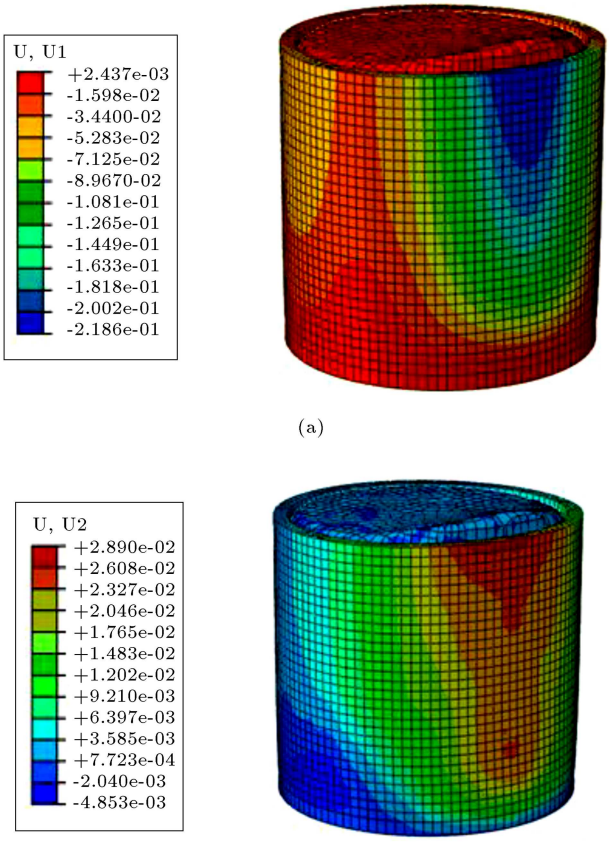

Figure 10. (a) Horizontal displacement contour (U1) of the water tank wall. (b) Vertical displacement contour of the water tank wall (U2).

is node-to-node. These nodes have displacements as pressure on the water tank following the explosion. The diagrams are examined from the water height inside the water tank and the dimensions of the water tank.

5.1.1. Evaluation of the water tank displacement based on the percentage of water filled

The water filling percentage effect has been investigated on the water tank wall displacements caused by the blast waves. Figure 10 demonstrates the contour of

the horizontal and vertical displacements of the water tank under blast loads. As shown in this figure, the highest displacement is concerned with the highest point of the water tank. The contours illustrate the maximum horizontal and vertical displacements of 21 and 2 cm, respectively. Every diagram in Figure 11 shows that if the water in the water tanks is exposed to the blast waves, it significantly affects the water displacement of the tank body. The pressure of the blast waves excites the water tank wall inwards, and the water pressure from the inside out opposes this explosive excitement. These diagrams show that the higher water height inside the water tank results in the lower inward displacement of the water tank wall. The blast waves hit the middle of the water tank. Thus, the displacement has been analyzed in this section of the water tank. Figure 11(a) demonstrates that the inward displacements occur at the height of 2 m from the water tank (the place where the blast waves hit). These displacements increase the upwards and decrease the downwards of the water tank base. The empty water tank has the highest displacement compared to other water tanks.

5.1.2. *Evaluation of water tank displacement based on H/R ratio*

In this section, the effect of the height to radius ratio on the body displacement to radius ratio of the water tank is discussed. Figure 11(a)-(c) show that water tanks with a more considerable height to radius ratio have a larger displacement to radius ratio. The $(H/R = 4/3)$ water tank has a smaller displacement to the radius ratio in the middle of the water tank body than $(H/R = 6/3)$ and $(H/R = 8/3)$ water tanks.

The height of the water tank makes it unstable against blast loads. The height to radius ratio of the water tank from the middle of the water tank to its base has a negligible effect on the displacement ratio of the water tank radius. However, the displacement ratio to the water tank radius varied significantly from the middle of the body height to the water tank base. The highest ratio of displacement to the radius of the water tank body $(H/R = 4/3)$ occurred at the upper edge of the water tank. However, in $(H/R = 6/3)$ and $(H/R = 8/3)$ water tanks, the highest ratio of displacement to radius is created in the middle of the body height.

5.1.3. *Evaluation of hoop stresses created in the water tank body*

The water tank is subjected to two factors after the explosion: a pressure wave caused by the explosion from the outside and pressure induced by water from the inside. According to the theory of Hausner, the water tank fluid is divided into the hard part and the wavy mass [4]. The leading cause of hoop stress is the

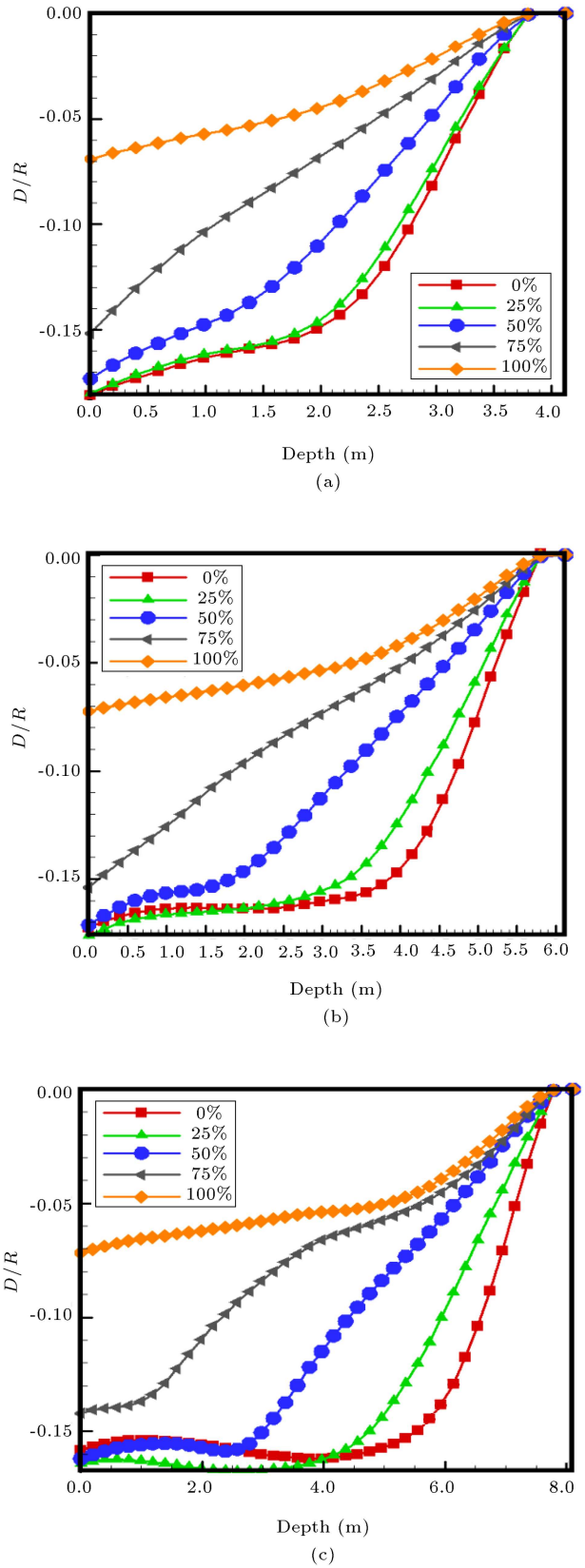

Figure 11. The ratio of body displacement to the water tank radius with respect to the water tank depth: (a) $(H/R = 4/3)$ water tank, (b) $(H/R = 6/3)$ water tank, and (c) $(H/R = 8/3)$ water tank.

wavy part of the water. If the water tank is 100% filled with water, the wavy section comprises a higher percentage of the total water. Thus, the resulting hoop stresses become more visible. The above diagrams reveal that the highest hoop stress occurs when it is 100% filled with water. These stresses are mitigated by reducing the filling percentage from 75 to 50 and from 25 to 0. The diagrams indicate that water in the tanks can affect the amount of hoop stress.

5.2. Evaluation of hoop stresses based on the percentage of water filled

The hoop stress diagrams of the water tank wall are observed along a path selected adjacent to the water tank wall under the blast pressure (path AB in Figure 9). The hoop stresses of this part of the water tank are plotted considering the selected nodes and using Figures 11 to 16. Also, the horizontal and vertical dimensions indicate the depth of the water tank and the hoop stresses, respectively. Figures 11 to 16 illustrate the hoop stress in the water tank wall caused by the blast. Also, these diagrams consist of three variables: (a) The percentage of water filling in the water tank (i.e., 0%, 25%, 50%, 75%, and 100%), (b) the explosion distance (i.e., 5 and 10 m), and (c) The height of the water tank (i.e., 4, 6, and 8 m). The hoop stresses generated in the water tank wall have a significant impact on the hoop stresses. The top to the bottom of the water tank is chosen to display the hoop stresses

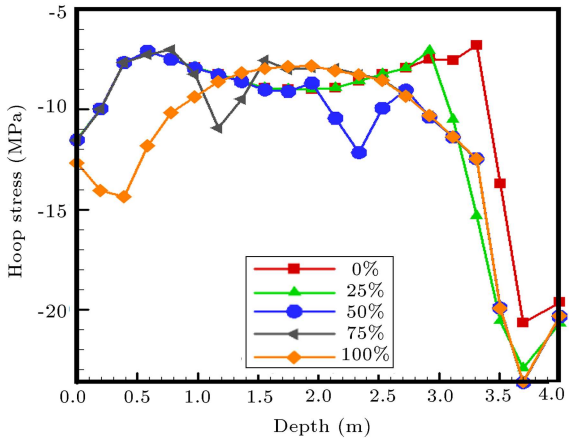

Figure 12. Hoop stresses ($H/R = 4/3$) with a blast distance of 5 m.

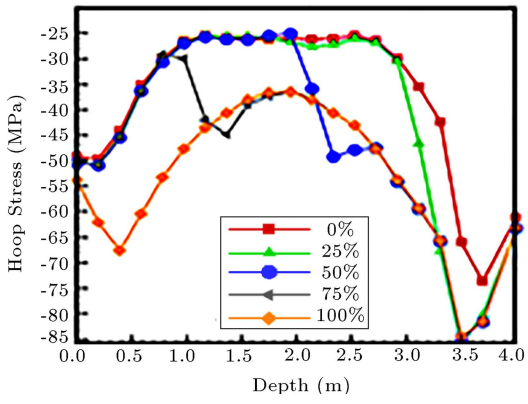

Figure 13. Hoop stresses ($\frac{H}{R} = 4/3$) with a blast distance of 10 m.

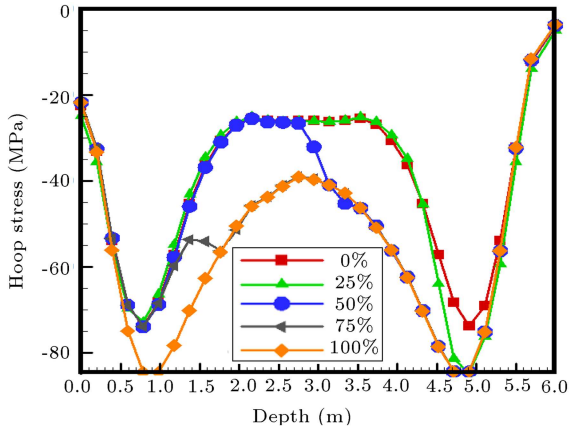

Figure 14. Hoop stresses ($H/R = 6/3$) with a blast distance of 5 m.

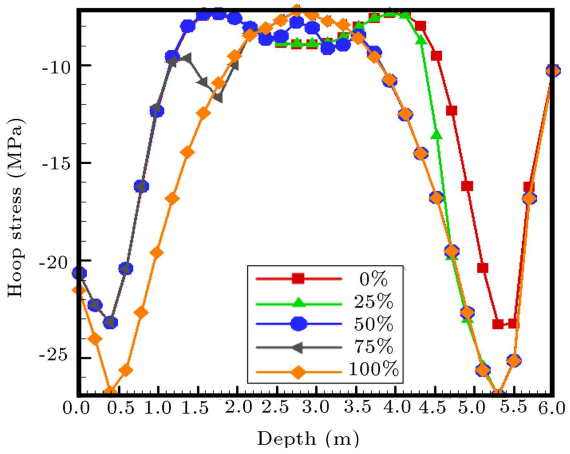

Figure 15. Hoop stresses ($H/R = 6/3$) with a blast distance of 10 m.

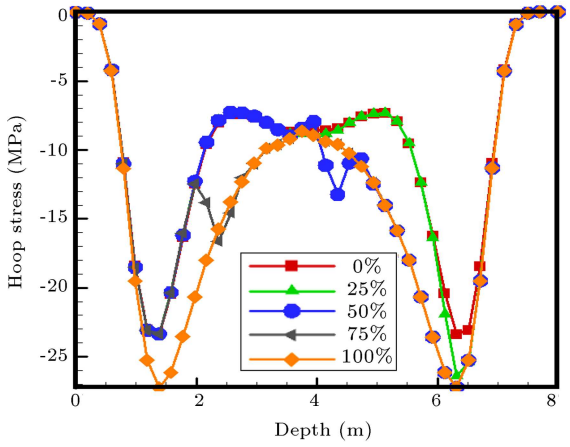

Figure 16. Hoop stresses ($H/R = 8/3$) with a blast distance of 5 m.

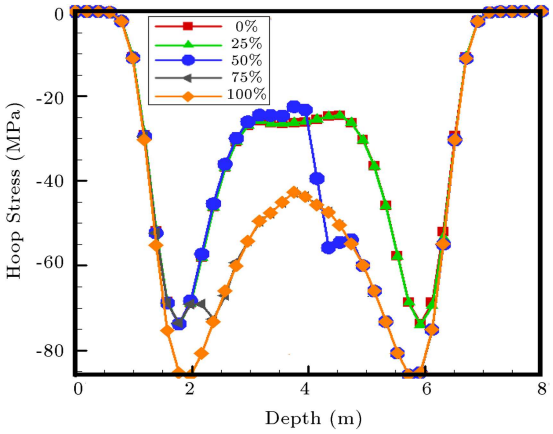

Figure 17. Hoop stresses ($H/R = 8/3$) with a blast distance of 10 m.

for the blast load. The blast waves are located in the middle of the water tank body.

5.3. Evaluation of hoop stresses based on the distance of explosives from the water tank

In general, a severe impulse is exerted on the back of the water tank wall at the moment of explosion. As a result, the water tank wall moves inwards, and its upper part is damaged. The hoop stress under blast pressure has the maximum value in the upper part of the water tank. Figures 12 to 17 show that if the blast distance changes from 5 to 10 m, the hoop stresses decrease by an average value of about 87.5% in all water tanks.

5.4. Hoop stresses evaluation based on ratio (H/R)

In this section, Figures 12 to 17 display that the H/R ratio effect can be observed on the hoop stresses of the water tank wall. This ratio is ineffective in the middle of the water tank wall exposed to the blast waves. Also, it does not reduce the stress. However, the blast wave distributions on the wall and the wave movements to the upper and lower parts of the water tank reduce their power and hoop stress. Since the blast load hits the middle of the water tank wall, the upper and lower parts of the water tanks with a higher H/R ratio have the least hoop stress. The diagrams show that all water tanks have the same hoop stresses in the middle of the wall height, while the hoop stresses in the upper and lower parts change. Therefore, the water tanks with the ratios of $H/R = 4/3$, $H/R = 6/3$, and $H/R = 8/3$ have the upper hoop stresses of 55, 22, and zero MPa, respectively.

5.5. Evaluation of the pressure on the water surface

In this section, Figures 18 to 23 exhibit the pressure created on the fluid surface after an explosion. The pressure created in the fluid surface elements occurs due to the blast loading on the water tank wall and

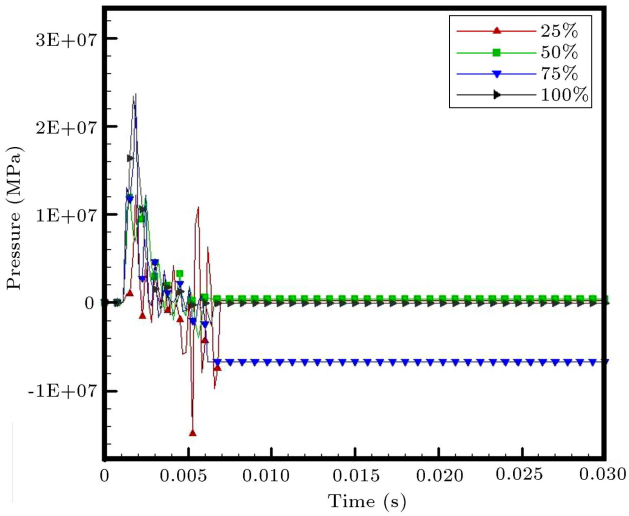

Figure 18. Water surface pressures ($H/R = 4/3$) at an explosion distance of 5 m.

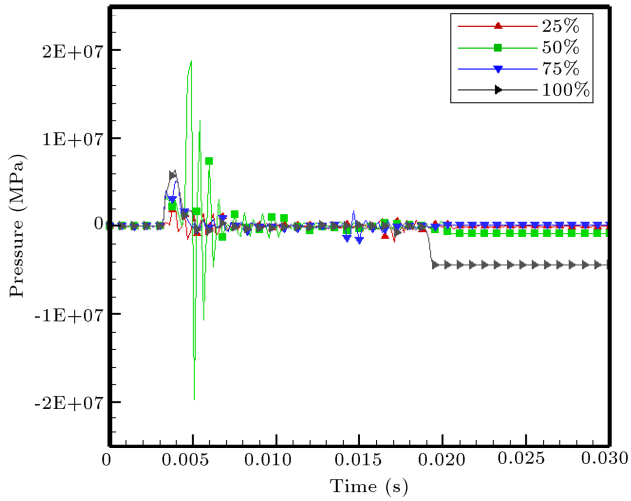

Figure 19. Water surface pressures ($H/R = 4/3$) at an explosion distance of 10 m.

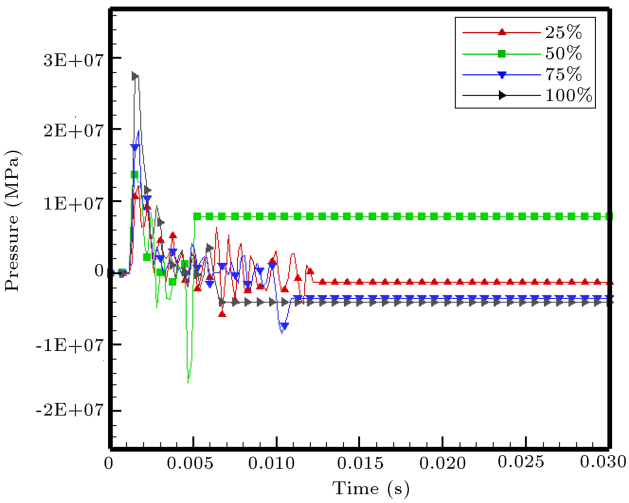

Figure 20. Water surface pressures ($H/R = 6/3$) at an explosion distance of 5 m.

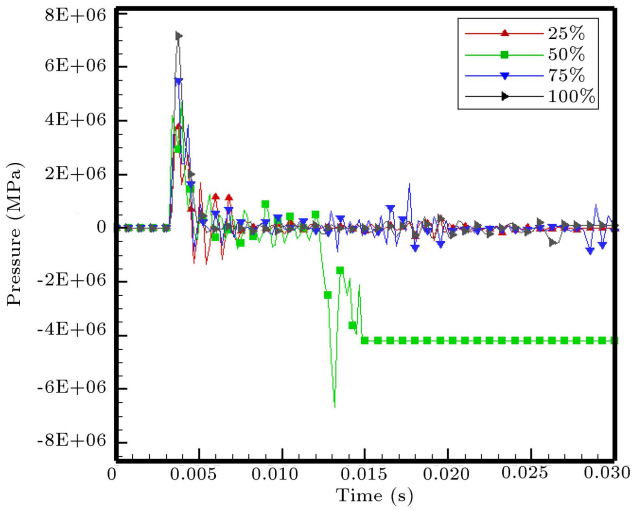

Figure 21. Water surface pressures ($H/R = 6/3$) at an explosion distance of 10 m.

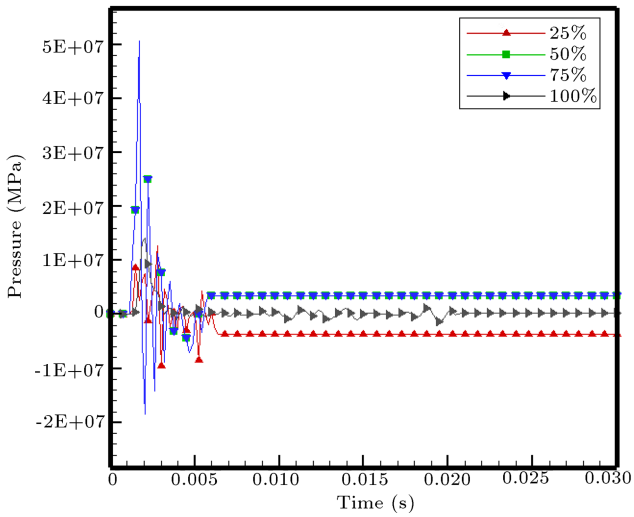

Figure 22. Water surface pressures ($H/R = 8/3$) at an explosion distance of 5 m.

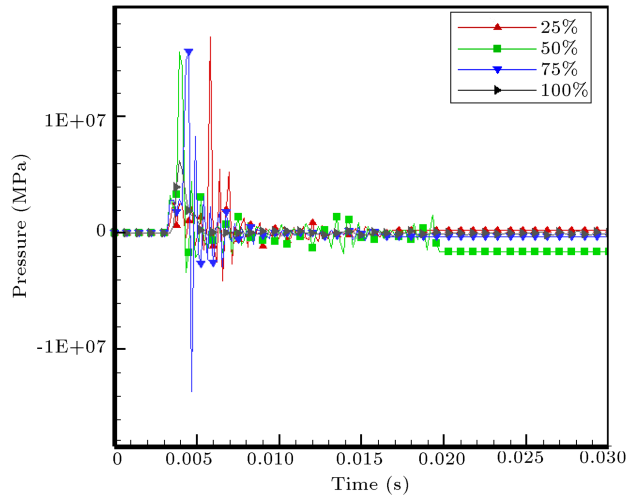

Figure 23. Water surface pressures ($H/R = 8/3$) at an explosion distance of 10 m.

the fluid-wall interaction inside the water tank. This type of pressure occurs in the fluid of water tanks with various heights and percentages of water filling. Also, the distances from the blast source to the water tank wall have a variety of diagrams. Each of these figures (i.e., 18 to 23) indicates water surface pressure diagrams over time.

5.6. Evaluation of the water surface pressure based on the filling percentage

The fluid stored in the water tanks causes turbulence on the fluid surface because of the explosion waves reaching the water tank wall and the exiting fluid-structure interaction. Also, the water tank is subjected to the pressure waves created by the explosion outside the water tank and the water pressure created inside the water tank. The theory of Hausner reveals that the fluid inside the water tank is divided into the hard part and the wavy mass [4]. Most of the fluid pressure occurs in the wavy mass. Since the blast load hits the middle of the tank height wall, water tanks containing 50% fluid have more pressure than the others. This issue is due to the exposure of the fluid surface to explosion waves.

5.7. Evaluation of the water surface pressure based on the distance of explosives from the water tank

In general, if the blast waves reach the water tanks, their intensity decreases based on their travel distance to the wall. This situation directly affects the water pressure inside the water tank. Figures 18 to 23 illustrate that the water surface pressure due to the explosion at a distance of 5 m has almost doubled compared to 10 m (i.e., on average, it has increased by about 10 MPa).

5.8. Evaluation of water surface pressure based on the (H/R) ratio

According to Figures 18 to 23, the effect of the H/R ratio is observed on the water surface pressure. This ratio has a maximum value at the beginning of the explosion moment and then decreases over time. Also, its pressure goes to zero. Since an increase in the height of the water tanks leads to the increment of the storage space, water tanks with a higher H/R ratio store more fluid and have more waves. Besides, an increase in the wavy water surface transfers more energy from the wall to the fluid. As a result, the water surface shows more pressure. The water surface pressure of the water tank with the $H/R = 8/3$ ratio is 50% higher than the water tank with the $H/R = 6/3$ ratio. Furthermore, the water surface pressure in the water tank with a H/R ratio of 6/3 is 33% higher than in the water tank with a H/R ratio of 4/3.

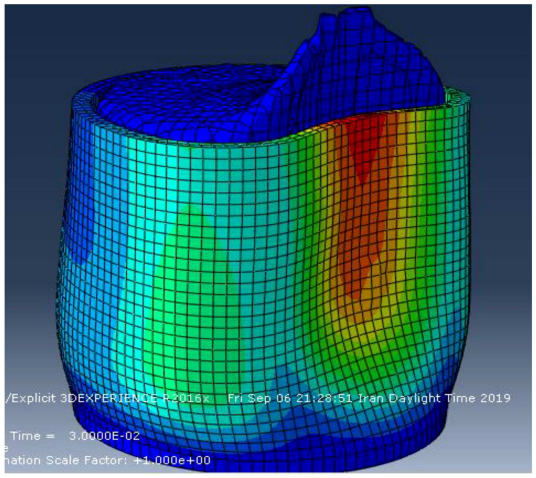

Figure 24. Turbulence of the tank water due to blast waves hitting the water tank wall.

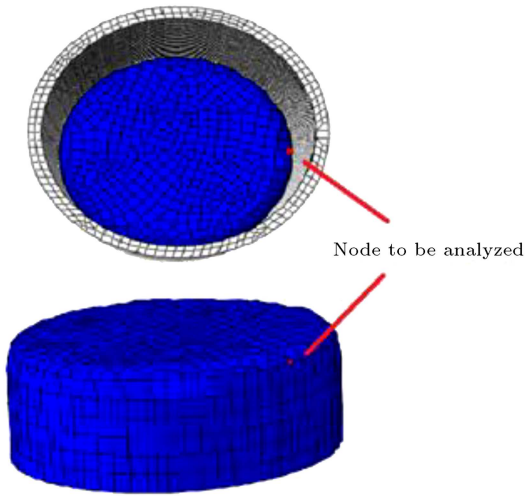

Figure 25. Fluid surface node.

5.9. Evaluation of fluid uplift in the water tank due to explosion

Water strikes the inner wall of the water tank because of the turbulence phenomenon, and some waves are formed on the water surface. The waves move horizontally and vertically, and then they are thrown out in open-top water tanks. Figure 24 demonstrates that a force is generated inside the water tank by hitting the water into the water tank wall, and subsequently, the water tank exerts a reciprocal force. The waves that excite the wall horizontally with their hydrodynamic force prevent the inward displacement of the water tank. The explosion increases the pressure inside the water tank, and the water also resists this pressure through hydrodynamic force and protects the water tank from possible damage. In open-top water tanks, vertical waves of water move outward.

5.10. Evaluation of fluid wave height with water element nodes

In this section, the water tank with the ratio of $H/R = 8/3$ and various filling percentages is studied. In this case, a node is chosen from the fluid on the blastexposed wall. This node is almost at the surface, and its movements are examined during the explosion. It represents various movements as a paradigm of the fluid surface. Indeed, it indicates the height of the fluid waves caused by the blast waves on the water tank wall and the water-structure interaction. Figure 25 depicts the fluid surface node, which varies with the percentage of the tank filling.

Also, Figures 26 to 29 show the fluid oscillation direction by the end of the explosion. In this case, water tanks filled with 50 and 100% fluid threw water up to a height of 2.5 m, and water tanks filled with 25 and 75% of the fluid threw water up to 1.5 m. Also, this deviation arises from the difference between the water level and the point of the blast waves'

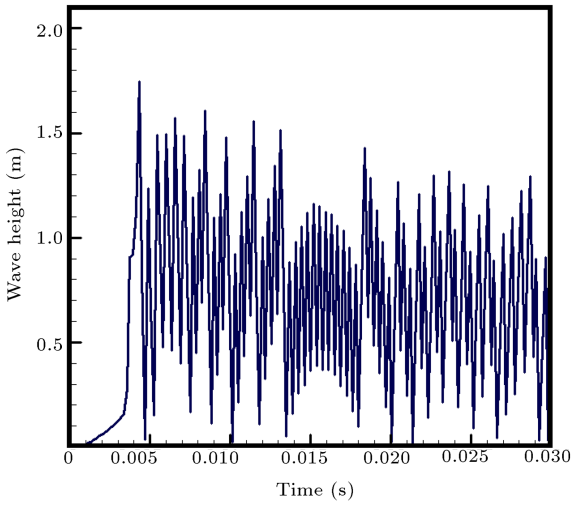

Figure 26. Displacement of node no. 8414 of water ($H/R = 8/3$) with 25% water filling at 10 m explosion distance.

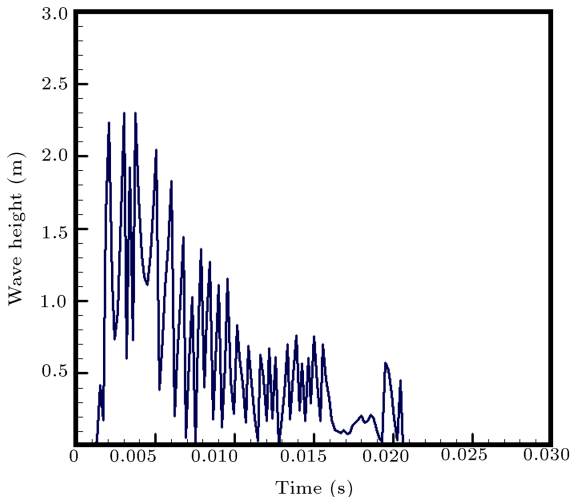

Figure 27. Displacement of node no. 17397 of water ($H/R = 8/3$) with 50% water filling at 10 m explosion distance.

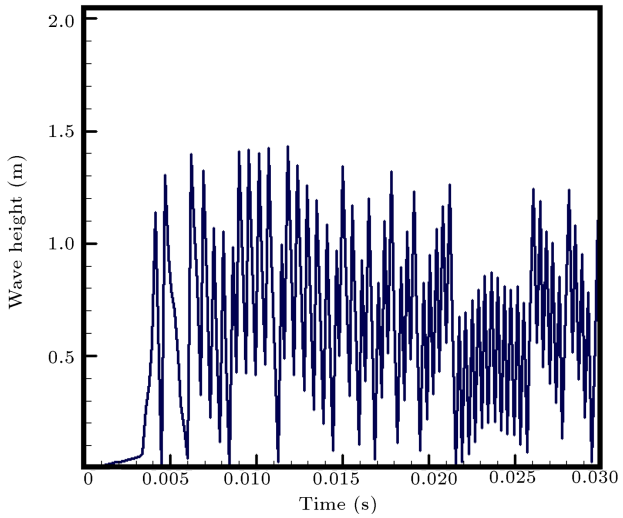

Figure 28. Displacement of node no. 24947 of water ($H/R = 8/3$) with 75% water filling at 10 m explosion distance.

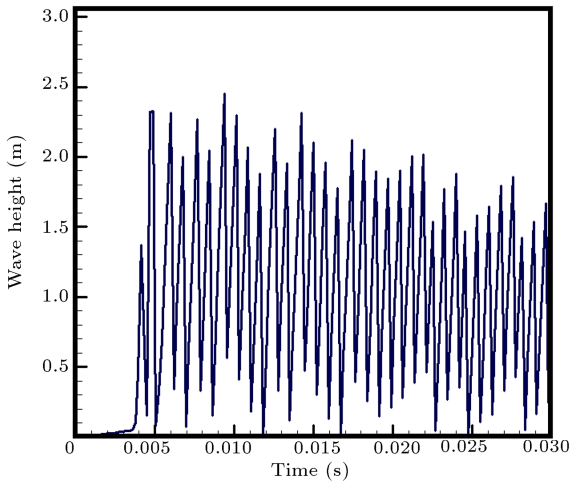

Figure 29. Displacement of node 34168 of water ($H/R = 8/3$) with 100% water filling at 10 m explosion distance.

impulse. Since the blast waves hit the center of the water tank wall, they stimulate the fluid at the back of the wall through the fluid-structure interaction. This situation causes displacements in the fluid. Besides, these displacements can be observed by the nodes of each element. It is essential to note that the nodes are arbitrarily chosen. Also, the concordance between the results does not necessarily exist because each node of water exhibits a unique behavior during explosion analysis, which is unpredictable. It is not possible to have an exact judge regarding the other nodes.

6. Conclusion

This study investigates the dynamic response of the reinforced concrete water tanks under specific blast loads. The results show that the parameters of water filling rate, water tank height to radius ratio, and distance from the blast center all have a significant impact on the dynamic response of the water tank structure. Indeed, the horizontal displacements increase by decreasing the water filling percentage and increasing the height of water tanks. Also, hoop stresses increase by enhancing the water volume. Also, these stresses are decreased by increasing the distance between explosives and the height of water tanks. The most remarkable outcomes of this study are expressed as follows:

- The presence of fluid in the water tank leads to pressure generation inside the water tank (due to the increasing hardness of the water tank) and reduces the explosion pressure from 10 to 20 MPa;
- A higher height to radius ratio represents the stability of sensitivity in the water tanks. It is essential to place a higher percentage of fluid in these water tanks to control their stability with increasing hardness;
- Most of the created strains appear above the water surface so that water tanks can block the body movement inward via hydrodynamic forces;
- The hoop stresses of the water tank body are created by the explosion waves outside of the water tank and the water pressure inside the water tank. The presence of water in the water tanks intensifies hoop stresses by an average of about 20 MPa;
- If the height of the water tanks increases, the hoop stresses in the upper and lower parts tend to zero;
- If the most compressive damage caused by the blast waves is applied to non-fluid points, it is necessary to consider these points for reinforcement;
- It is essential to consider water tank reinforcement ideas on the blast side due to the further damage.

References

1. "Criteria for design and calculation of groundwater reservoirs", *Journal of the Office of Technical Affairs and Development of Criteria of the Management and Planning Organization*, **123**.
2. Munson, B., Young, D., and Okiishi, T., Fluid Mechanics, Wiley (2016).
3. Yazdanian, M., Razavi, S.V., and Mashal, M. "Seismic analysis of rectangular concretewater tanks by considering fluid and tank interaction" , *Journal of Solid Mechanics*, **8**(2), pp. 435–445 (2016).
4. Djermane, M., Zaoui, D., Labbaci, B., et al. "Dynamic buckling of steelwater tanks under seismic excitation: numerical evaluation of code provisions", *Engineering Structures*, **70**, pp. 181–196 (2014).

5. Yazdanian, M., Mashal, M., and Razavi, S.V. "Seismic vulnerability of cylindrical steel liquid storagewater tanks for an oil industry plant ", *Anadolu University Journal of Science and Technology A*, **18**(2), pp. 275–288 (2017).

6. Yazdanian, M., Razavi, S.V., and Mashal, M. "Study on the dynamic behavior of cylindrical steel liquid storage tanks using finite element method", *Journal of Theoretical and Applied Vibration and Acoustics*, **2**(2), pp. 145–166 (2016).

7. Hoskins, L.M. and Jacobsen, L.S. "Water pressure in a tank caused by simulated earthquake", *Bull. Seismological Soc. Am.*, **24**, pp. 1–32 (1934).

8. Housner, G.W.W., *Dynamic pressures on accelerated fluid containers*, Bulletin of the Seismological Society of America, pp. 15–35 (1957).

9. Epstein, H.I. "Seismic design of liquid storage tanks", *J. Struct. Division-ASCE*, **102**, pp. 1659–1673 (1976).

10. Haroun, M.A.A., *Dynamic Analyses of Liquid Storage Tanks*, EERL, pp. 80–104 (1980).

11. Veletsos, A.S. "Seismic response and design of liquid storagewater tanks", *Guidelines for the Seismic* (1984).

12. Buratti, N. and Tavano, M. "Dynamic buckling and seismic fragility of anchored steel tanks by the added mass method", *Earthquake Eng Struct Dynam*, **43**(1), pp. 1–21 (2014).

13. Ruiz, R.O., Lopez-Garcia, D., and Taflanidis, A.A. "An efficient computational procedure for the dynamic analysis of liquid storage tanks", *Engineering Structures*, **85**, pp. 206–218 (2015).

14. Javanmardi, M., Binns, J., Thomas, G., et al. "An investigation into the effect of pressure source parameters and water depth on the wake wash wave generated by moving pressure source", *Scientia Iranica*, **25**(4), pp. 2162–2174 (2018).

15. Zhang, H., Liu, L., He, X., et al. "Investigation of wind-induced response of fluid-solid coupling system for high bent-type aqueduct", *Scientia Iranica*, **25**(1), pp. 50–64 (2018).

16. Brunesi, E., Roberto, N., Marco, P., et al. "Seismic performance of storage steel tanks during the May 2012 Emilia, Italy, earthquakes", *Journal of Performance of Constructed Facilities*, **29**(5) (2015).

17. Colombo, J.I. and Almazán, J.L. "Seismic reliability of continuously supported steel wine storage tanks retrofitted with energy dissipation devices", *Engineering Structures*, **98**, pp. 201–211 (2015).

18. Jin, H., Calabrese, A., and Liu, Y. "Effects of different damping baffle configurations on the dynamic response of a liquid tank under seismic excitation", *Engineering Structures*, **229**, pp. 201–211 (2021).

19. US Department of Army, the Navy, and Air Force. "The design of structures to resist the effects of accidental explosions", TM 5-1300. Washington DC: NAVFAV P-397. 559-920 (1990).

20. Stein, L.R., Gentry, R.A., and Hirt, C.W. "Computational simulation of transient blast loading on three-dimensional structures", *Comput. Methods Appl. Mech. Eng.*, **11**, pp. 57–74 (1977).

21. Baumbach, M.R. "Design of metal hollow section tubular columns subjected to transverse blast loads", *Thin-Walled Struct*, **68**, pp. 92–105 (2013).

22. Wang, Y., Liew J.Y.R., and Lee, S.C. "Structural performance of tank under static and dynamic pressure loading", *Int J Impact Eng.*, **85**, pp. 110–23 (2015).

23. Mittal, V., Chakraborty, T., and Matsagar, V. "Dynamic analysis of liquid storage tank under blast using coupled Euler-Lagrange formulation", *Thin-Walled Struct*, **84**, pp. 91–111 (2014).

24. Hu, K. and Zhao, Y. "Numerical simulation of internal gaseous explosion loading in large-scale cylindrical tanks with fixed roof", *Thin-Walled Structures*, **105**, pp. 16–28 (2016).

25. Zhang, R.L., Jia, J.J., Wang, H.F., et al. "Shock response analysis of a large LNG storage tank under blast loads", *KSCE Journal of Civil Engineering*, **22**(9), pp. 3419–3429 (2018).

26. Li, J., Hao, H., Shi, Y., et al. "Experimental and computational fluid dynamics study of separation gap effect on gas explosion mitigation for methane storager tanks", *Journal of Loss Prevention in the Process Industries*, **55**, pp. 359–380 (2018).

27. Li. J. and Hao, H. "Far-field pressure prediction of a vented gas explosion from storage tanks by using new CFD simulation guidance", *Process Safety, and Environmental Protection*, **119**, pp. 360–378 (2018).

28. Shengzhou, L., Wang, W., Weidong, C., et al. "Behaviors of thin-walled cylindrical shell storage tank under blast impacts", *Shock and Vibration*, pp. 1–23 (2019).

29. Yasseri, S. "Blast pressure distribution around large storage tanks", *Blast information Group*, **67**, pp. 133–134 (2015).

30. Safa, P. "Investigation of explosion effect on the groundwater tank with a floating roof ", *Scientific Journal of Passive Defense*, **6**(1), pp. 13–24 (2015) (In Persian).

31. Yonghui, W. and Hongyuan, Z. "Numerical study of water tank under blast loading", *Thin-Walled Structures*, **90**, pp. 42–48 (2015).

32. *Abaqus/Explicit User's Manual, Version*, Dassault Systems
Simulia Corporation, Providence, Rhode Island, USA (2016).

33. Hafez, A. "Seismic response of ground-supported circular concrete tanks", Ph.D. Thesis, Graduate School of Ryerson University (2012).

34. Johnson, G.R. and Cook, W.H. "Fracture characteristics of three metals subjected to various strains, strain rates, temperatures, and pressures", *Int JFract Mech.*, **21**, pp. 31–48 (1985).

35. Luccioni, B., Ambrosini, D., Danesi, R. "Blast load assessment using hydrocodes", *Eng. Struct*, **28**, pp. 1736–1744 (2006).

Biographies

Majid Moghadam is a master student in Hydraulic Structure at the Jundi-Shapur University of Technology, Dezful, Iran. His supervisors are Dr. Vahid Razavi and Mehrdad Sharbanuzadeh. His main area of research includes Hydraulic Structures, Smart Structures, Reinforced Concrete Elements, and Numerical Methods in Engineering.

SeyedVahid Razavitosee is an Assistant Professor in the Structural Engineering Department of the Jundi-Shapur University of Technology, Dezful, Iran. His main area of research includes Reinforced Concrete and Steel Structures, Neural Networks, Concrete Technology, and more recently dynamic assessment and health monitoring of bridge.

Mehrdad Shahrbanouzadeh is an Assistant Professor in the Water Engineering Department of the Jundi-Shapur University of Technology, Dezful, Iran. His main area of research includes numerical methods in engineering (finite element method, finite difference method, isogeometric analysis), hydraulic structures (concrete dam, earth dam), and environmental and water resources (numerical and experimental models in groundwater, coastal aquifers).